The Local Last Glacial Maximum of the southern Scandinavian Ice Sheet front: Cosmogenic nuclide dating of erratics in northern Poland

Karol Tylmann, Vincent Rinterknecht, Piotr Woźniak, Didier Bourles, Irene Schimmelpfennig, Valery Guillou, Georges Aumaitre, Karim Keddadouche

The Local Last Glacial Maximum of the southern Scandinavian Ice Sheet front: cosmogenic nuclide dating of erratics in northern Poland

Karol Tylmann[1*], Vincent R. Rinterknecht[2], Piotr P. Woźniak[1], Didier Bourlès[3], Irene Schimmelpfennig[3], Valery Guilou[3], ASTER Team[3a]

[1] University of Gdańsk, Faculty of Oceanography and Geography, Poland (k.tylmann@ug.edu.pl)

[2] Université Paris 1 Panthéon-Sorbonne, Laboratoire de Géographie Physique, CNRS, UMR 8591, France,

[3] Aix Marseille Université, CNRS, IRD, INRA, Coll France, CEREGE, Aix-en-Provence, France

* Corresponding author

[a] Georges Aumaître, Karim Keddadouche

Abstract

This paper presents new results of terrestrial cosmogenic nuclide dating of erratics in northern Poland. We report the first exposure ages of erratics located on the pre-Local Last Glacial Maximum and the Local Last Glacial Maximum moraines in Poland. Published radiocarbon ages are calibrated and used as a background indicator of the possible time window for the Local Last Glacial Maximum.

The terrestrial cosmogenic nuclide exposure ages presented in this study indicate that: (1) exposure ages of erratics located on the pre-Local Last Glacial Maximum moraines (15.9 ± 1.4 to 101.7 ± 8.5 ka) are not clustered around any specific time interval, (2) the age of the ice-sheet retreat from the Local Last Glacial Maximum ice limit in western Poland is 20.7 ± 0.8 ka and the probable duration of the Local Last Glacial Maximum in western and central Poland is between ~25 ka and ~21 ka, (3) the age of the ice sheet retreat from the Local Last

25 Glacial Maximum ice limit in eastern Poland is 17.3 ± 0.5 ka and the probable duration of the
26 Local Last Glacial Maximum in eastern Poland is between ~22 ka and ~18 ka. Our results
27 show that the Local Last Glacial Maximum ice limit in western and central Poland is probably
28 ~3 ka older than in eastern Poland. This support a scenario for a complex response of the last
29 Scandinavian Ice Sheet southern margin to the climatic fluctuations and/or to internal
30 dynamics of the ice sheet.

31 **Key words**: Local Last Glacial Maximum, Leszno (Brandenburg) Phase, Poznań (Frankfurt
32 Phase), cosmogenic nuclide dating, Scandinavian Ice Sheet, erratics.

33 1. Introduction

34 The Last Glacial Maximum (LGM) is defined as the most recent period with the
35 maximum global integrated volume of ice sheets and the corresponding minimum global sea
36 level (Mix et al., 2001; Clark et al., 2009; Hughes et al., 2013) and dated to 23–19 cal ka BP
37 or 24–18 cal ka BP (cf. Mix et al., 2001; Hughes and Gibbard, 2015). The termination of the
38 LGM climatic cooling resulted in the progressive shrinking of the inland ice, which for most
39 of the Northern Hemisphere ice sheets is dated at ~20–17 ka (Hughes and Gibbard, 2015).
40 However, numerical ages (based on calibrated ^{14}C, terrestrial cosmogenic nuclides – TCN or
41 luminescence dating) of terrestrial deposits show significant regional variability in the timing
42 of the ice sheets' maximum extent and the commencement of their retreat. Most of the ice
43 sheets reached their maximum extents in a 7.0 ka time interval between 26.5 ka and 19.0 ka
44 (Clark et al., 2009), but the maximum extents of specific ice sheets (Local Last Glacial
45 Maxima – LLGM) were found to be asynchronous and not always in agreement with the
46 global LGM (Hughes et al., 2013).

47 The Scandinavian Ice Sheet (SIS) was one of the main Northern Hemisphere ice sheet
48 and covered a significant part of northern Europe during the LGM. Timing of the last SIS

maximum expansion and retreat is important to understand climatic fluctuations at the end of the Marine Isotope Stage (MIS) 2. The LLGM to the south of the Baltic Basin (Fig. 1A) is dated at ~24 ka in Germany and western Poland, and at ~19 ka in eastern Poland based on calibrated ^{14}C and OSL ages (Marks, 2012 after Stankowska and Stankowski, 1988; Wysota et al., 2009) and at 21–19 ka in Belarus and Lithuania based on calibrated ^{14}C and ^{10}Be ages (Rinterknecht et al., 2007, 2008). Thus, the maximum extent of the of the last SIS in Poland was probably asynchronous with earlier maximum expansion of the ice sheet in western and central Poland and subsequent maximum expansion further to the east (Fig. 1A and B). Nevertheless, there is still a relatively small number of geochronological data constraining the timing of LLGM in north Poland. Specifically, there is a lack of direct dating (TCN) of moraines correlated with the maximum limit of the last ice sheet in this region.

Here we present a new set of TCN exposure ages of erratic boulders located within the southern front of the last SIS in northern Poland. It provides the first exposure ages of erratics located on the pre-LLGM moraines and new exposure ages on the LLGM moraines in Poland. Additionally, published ^{14}C ages were calibrated with the most recent radiocarbon calibration curve and used as a background indicator of the possible time window for the LLGM. We discuss our results in a wider chronological context including specifically the growing number of luminescence ages available for the southern fringe of the last SIS (e.g. Houmark-Nielsen and Kjaer, 2003; Wysota et al., 2009; Lüthgens et al., 2011; Bitinas, 2012; Lasberg and Kalm, 2013), as well as existing reconstructions of the SIS evolution (e.g. Hughes et al., 2016; Stroeven et al., 2016). The objective of this paper is to date the asynchronous maximum extent of the last SIS in northern Poland based on new exposure ages, and on the extensive dataset of TCN exposure ages already published.

2. Study area

The study area is located in NW Poland and covers ~20% (~500 km) of the LLGM ice sheet margin south of the Baltic Sea. The investigated region is situated within the eastern part of the extensive, lobe-shaped fringe of the last SIS (Fig. 1A). The region is large enough to find a considerable number of erratics suitable for TCN exposure dating (Tylmann et al., 2018) and to track the last SIS retreat from its maximum limit.

The ice sheet limit of the LLGM in northern Poland is mostly based on the spatial distribution of end moraines, outlets of tunnel valleys or proximal parts of outwash plains and fans (Majdanowski, 1947; Galon and Roszkówna, 1961; Marks, 2002). This limit defines the "young glacial" landscape located to the north and the "old glacial" landscape located to the south of it (Fig. 1B). According to recent reconstructions, the LLGM was diachronous and it occurred during the Leszno/Brandenburg Phase in the western part and during the Poznań/Frankfurt Phase in the eastern part of the study area (Marks, 2011, 2012, 2015; Fig. 1B). It is supported by lithostratigraphic evidences which suggest asynchronous maxima of the last SIS across the study area. In north-central Poland two till layers separated by ice-wedge casts, are correlated with the glacial phases mentioned above (Wysota et al., 2009; Narloch et al., 2013). However, in the former Vistula Ice Lobe area (Fig. 1B), only one till layer has been identified, and OSL dating of fluvial and glaciofluvial sediments suggests that it is correlated with the Poznań Phase (cf. Wysota et al., 2009; Roman, 2017). In contrast, in the western part of the study area, the till layer correlated with the Leszno Phase occurs close to the maximum extent of the last SIS, and no basal till layer correlated with the Poznań Phase has been documented there. Therefore, the ice marginal belt formed during the Poznań Phase in western Poland is commonly interpreted as a result of the ice margin standstill, which occurred during the last SIS recession after the LLGM of the Leszno Phase (e.g. Kasprzak, 1988; Kozarski, 1988, 1995).

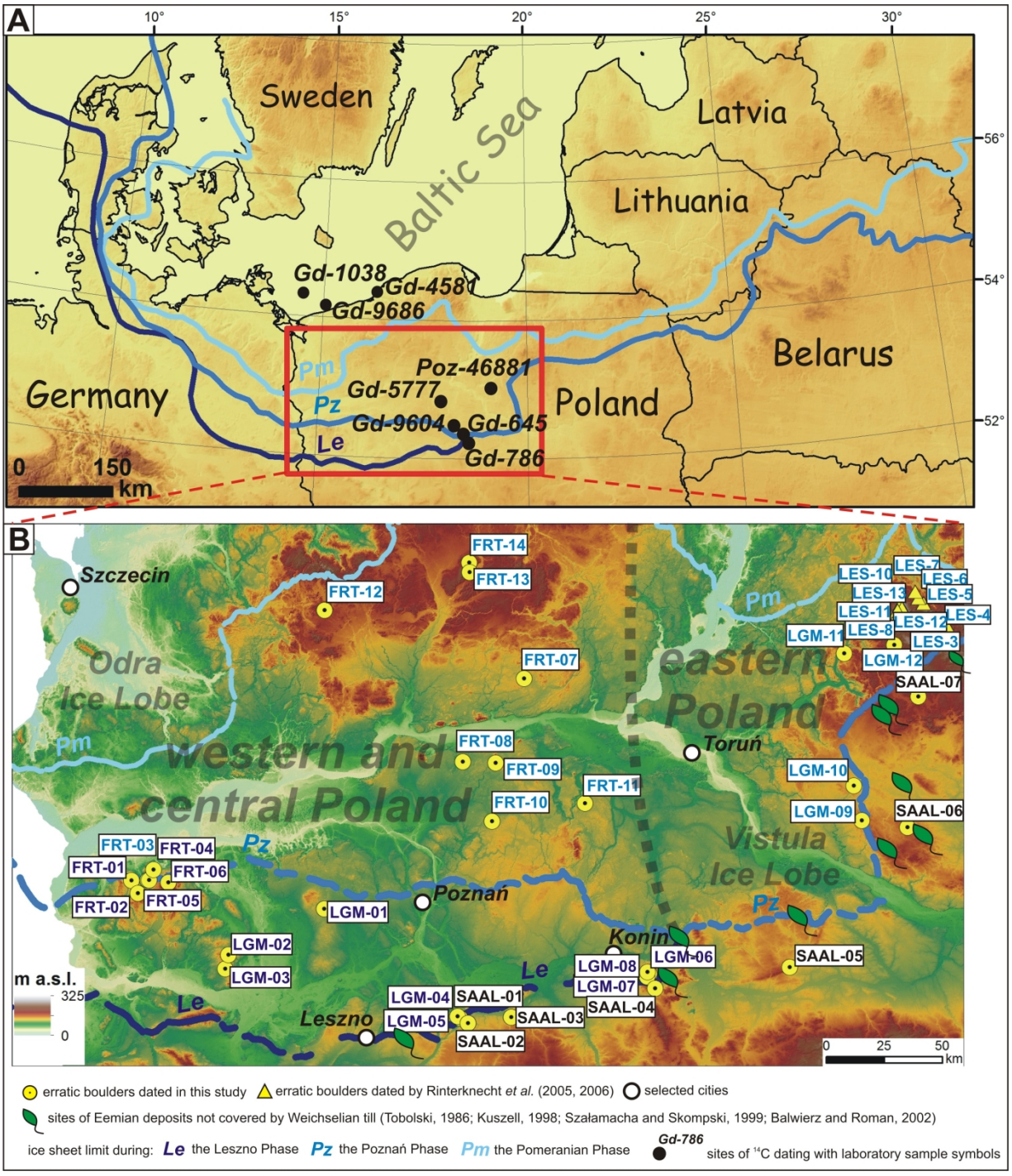

Fig. 1. The main ice margin limits of the last Scandinavian Ice Sheet (SIS) in the area south of the Baltic Sea and the study area with erratic boulders. (A) Location of the study area within the southern front of the last SIS. Dark dots indicate location of radiocarbon ages used in the article. (B) The location of erratic boulders dated with terrestrial cosmogenic nuclides (TCN). Limits of the last SIS from Marks et al. (2006) and Kozarski (1995).

Up until recently, the age of the maximum extent of the last SIS in the study area was interpreted mainly based on available radiocarbon ages (Table 1 and references therein). Published ^{14}C data significant for the interpretation of the last SIS advance and retreat (locations in Fig. 1A) indicate the possible time window for its maximum extent and the beginning of its retreat. Radiocarbon ages from organic deposits resting below the LLGM till layers have been obtained in the vicinity of the last SIS maximum limit in central Poland (Stankowska and Stankowski, 1988; Gogołek and Mańkowska, 1989) as well as in the area of the northern Polish coastline (Rotnicki and Borówka, 1995) and in offshore boreholes drilled into the Baltic Sea bottom (Kramarska, 1998; Krzyszkowski et al., 1999). The youngest calibrated radiocarbon ages of these deposits constrain the maximum reliable age of the LLGM. The most reliable ages for the ice sheet retreat, may be estimated by the oldest calibrated radiocarbon ages of the organic sediments deposited after deglaciation at the bottom of lake basins close to the last SIS maximum extent in central and northern Poland (Niewiarowski, 1995; Stankowski et al., 1999; Gamrat et al., 2017). Because of the risk of organic matter redeposition at the bottom of lake basins and the associated overestimated radiocarbon ages, these ages should be interpreted as a maximum reliable time interval for the deglaciation of north-central Poland after the LLGM.

The calibrated radiocarbon ages of organic deposits underlying the LLGM till layers range between 26.5 ± 1.3 and 25.2 ± 3.4 cal ka BP. The oldest minimum age predating the LLGM was found on the northern Polish coastline (Rotnicki and Borówka, 1995) and the youngest one in central Poland (Gogołek and Mańkowska, 1989). The post-LLGM maximum ages of organic sediments deposited after deglaciation range between 21.4 ± 1.9 cal ka BP and 19.1 ± 0.2 cal ka BP. The oldest age (21.4 ± 1.9 cal ka BP) from bottom part of the lake deposits resting above the LLGM till in central Poland (Stankowski et al., 1999). A similar age (21.4 ± 0.6 cal ka BP) was obtained from the bottom of the lacustrine deposits overlying

128 the till of the same stratigraphic position, ~60 km further to the north (Niewiarowski, 1995).
129 The youngest maximum post-LLGM age (19.1 ± 0.2 cal ka BP), was found in lacustrine silt
130 filling glacial channel located further to the east (Gamrat et. al., 2017).
131 The distribution of pre-LLGM and post-LLGM calibrated ^{14}C ages in the study area
132 suggests that:
133 1) the LLGM ice advance occurred after ~25 cal ka BP,
134 2) the beginning of ice sheet retreat after the LLGM in central-western Poland
135 occurred not earlier than ~21.5 cal ka BP and the deglaciation of the regions located
136 further to the east started not earlier than ~19.0 cal ka BP.

137 **3. Methods**

138 *3.1. Sample selection*

139 The largest erratic boulders located in situ on glacial landforms in the vicinity of the
140 maximum extent of the last SIS and to the north of this limit were our targets for sampling for
141 surface exposure dating with TCN (Fig. 1B). The boulders were carefully selected from an
142 extensive dataset of almost 500 erratics, based on their dimensions and geomorphological
143 locations (Tylmann et al., 2018). We selected erratics located on depositional glacial
144 landforms, i.e. terminal moraines, dead-ice moraines, moraine plateaux or proximal zones of
145 outwash fans/plains. Samples were collected with a manual jackhammer from the upper
146 surface of 33 stable and massive boulders of perimeter ranging from 6.0 to 14.3 m and of
147 height ranging from 0.8 to 2.9 m (Table 2; see examples in Fig. 2). Almost all boulders (n =
148 32) are characterized by quartz-rich lithologies – granitoid, granite gneiss and gneiss. Because
149 of the availability of quartz, these erratics were sampled for surface exposure dating with in
150 situ-produced ^{10}Be. Out of 33 samples for ^{10}Be analysis (Table 2), one boulder was sampled
151 twice; we took a sample from the top (LGM-02T) and one from the side (LGM-02S). The

motivation of this sampling was that from the field observations the boulder looked to have been rotated by 90°, with the original top surface on the side (Fig. 2C). One boulder does not contain quartz (gabbro) and it was sampled for exposure dating with in situ-produced ^{36}Cl (Fig.2D, Tables 3 –5). In total, 34 new samples were analyzed: 33 for ^{10}Be analysis and one for ^{36}Cl analysis.

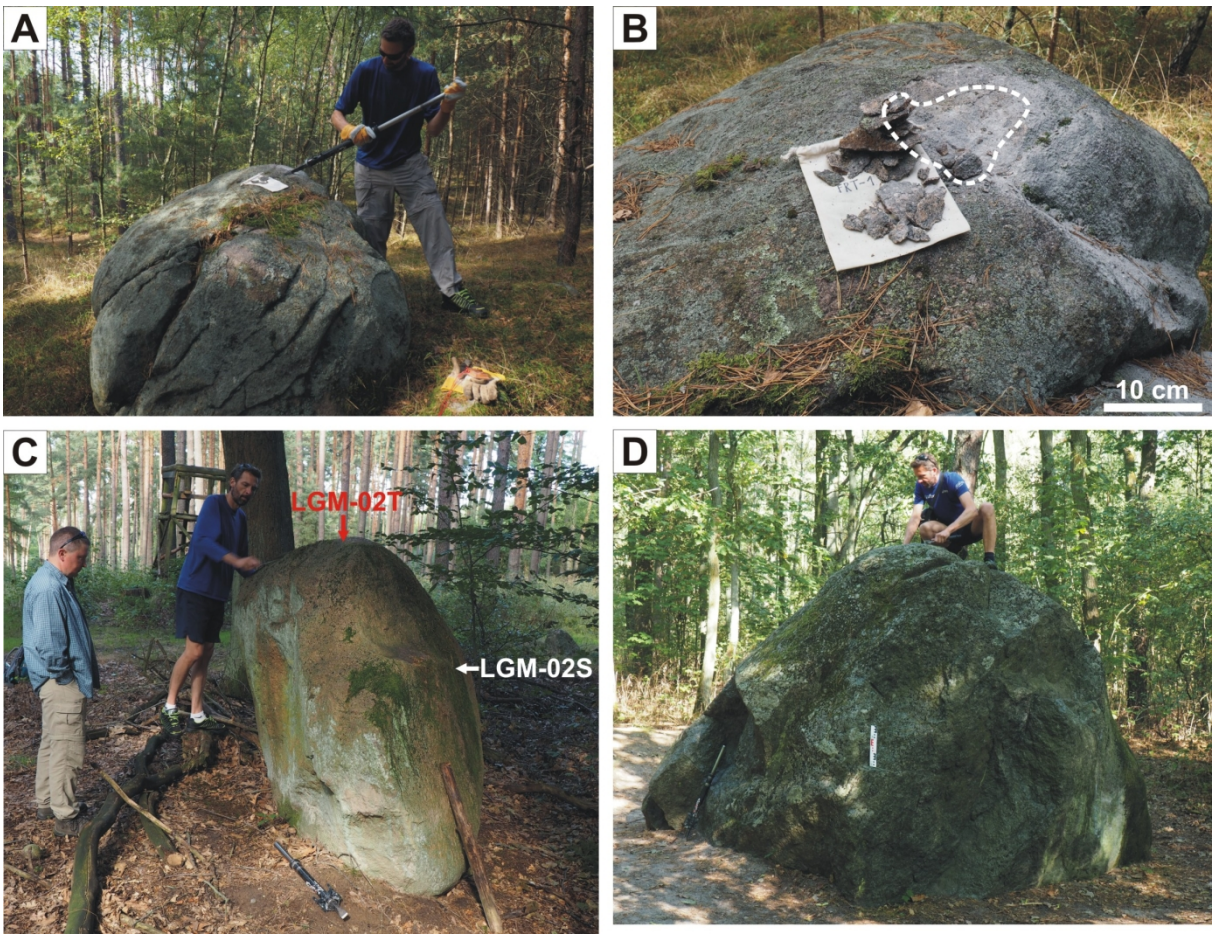

Fig. 2. Examples of erratic boulders sampled for TCN exposure dating. (A) Sampling of FRT-01 boulder upper surface with a manual jackhammer. (B) FRT-01 sampling spot with the scar (outlined by a white dashed line) and the collected material. (C) LGM-02 boulder, probably rotated 90° clockwise. Arrows show location of samples LGM-02T (present top of the boulder) and LGM-02S (hypothesized to be the original top). (D) FRT-11 boulder (gabbro); the only one sampled for ^{36}Cl.

3.2. ^{10}Be dating methodology

The samples were crushed and sieved. The 0.25–1.0 mm fraction was divided with a Frantz separator into magnetic and non-magnetic subsamples. The non-magnetic fractions were enriched in quartz decontaminated by successive acid leaching (HCl + H_2SiF_6 then dilute HF). The purified quartz was spiked with ~100–300 mg of a 3025 ppm home-made carrier then dissolved in 48% HF. After evaporation and purification with Dowex 1 X 8 and Dowex 50W * 8 (100-200 mesh) ion exchange resins, BeOH was dried and then oxidized to BeO at 800°C. BeO was mixed with 325 mesh Nb-powder prior to measurement at the accelerator mass spectrometer (AMS). Sample preparation was conducted at the Laboratoire National des Nucléides Cosmogéniques (LN_2C) at CEREGE, Aix-en-Provence, France. The French AMS facility ASTER was used for the ^{10}Be measurements (Arnold et al., 2010). The measured ^{10}Be/^{9}Be ratios were normalized relative to the in-house standard STD-11 using an assigned ^{10}Be/^{9}Be ratio of $(1.191 \pm 0.013) \times 10^{-11}$ (Braucher et al., 2015) and a ^{10}Be half-life of $(1.387 \pm 0.012) \times 10^{6}$ years (Chmeleff et al., 2010; Korschinek et al., 2010).

^{10}Be ages were calculated using the most recent global production rate (Borchers et al., 2016) and the 'Lm' time-dependent scaling scheme for spallation according to Lal (1991) and Stone (2000). The modern global ^{10}Be production rate at sea level and high-latitude is derived from a recalibrated global data set and recent calibration studies (Borchers et al., 2016). This production rate was used as the most adequate, because the local production rate for Poland was not estimated so far. A recently published Swedish ^{10}Be production rate (Stroeven et al., 2015) would generate slightly younger exposure ages (~5%). The ^{10}Be production rate was corrected for sample thickness according to an exponential function (Lal, 1991) and assuming an average density of 2.7 g/cm^3. A correction for self-shielding (direction and angle of surface dipping) was applied when the surface of a sampling spot was sloping >10°. However, for most of the sampled boulders no correction for surface inclination was necessary. We apply a

correction for surface erosion, assuming a maximum erosion rate of 1.3 mm ka^{-1} for granitic surfaces (Gosse et al., 1995; Rinterknecht et al., 2012, 2014). Corrections for snow/vegetation cover were not included due to their minimal impact on ^{10}Be ages in the temperate vegetation zone (e.g. Plug et al., 2007; Rinterknecht et al., 2014). All calculations were performed using the online exposure age calculator formerly known as the CRONUS-Earth online exposure age calculator – version 3 (http://hess.ess.washington.edu/math/; accessed: 2019-02-01), which is an updated version of the online calculator described by Balco et al. (2008). ^{10}Be exposure ages corrected and uncorrected for erosion are reported with 1σ uncertainties (including analytical uncertainties and the production rate uncertainty) in ka in Table 2. In the following sections we use ages uncorrected for the erosion and we interpret them as minimum ages for the ice sheet retreat.

3.3. ^{36}Cl dating methodology

Gabbro sample FRT-11 was crushed and sieved to a grain size fraction of 250–710 µm at CALM (Cosmonucléides Au Laboratoire de Meudon) at the Laboratoire de Géographie Physique (LGP), France, and chemically prepared for in situ ^{36}Cl dating at the LN_2C. The procedure is described in Schimmelpfennig et al. (2011). Sample specific data and compositional results are given in Tables 3, 4 and 5. The ^{36}Cl age of sample FRT-11 was calculated with the Excel® spreadsheet of Schimmelpfennig et al. (2009), using the scaling method of Stone (2000) and employing the following ^{36}Cl production rates, referenced to sea level and high latitude (SLHL): 42.2 ± 4.8 atoms ^{36}Cl $(g\ Ca)^{-1}$ yr^{-1} for spallation of Ca (Schimmelpfennig et al., 2011), 148.1 ± 7.8 atoms ^{36}Cl $(g\ K)^{-1}$ yr^{-1} for spallation of K (Schimmelpfennig et al., 2014), 13 ± 3 atoms ^{36}Cl $(g\ Ti)^{-1}$ yr^{-1} for spallation of Ti (Fink et al., 2000), 1.9 ± 0.2 atoms ^{36}Cl $(g\ Fe)^{-1}$ yr^{-1} for spallation of Fe (Stone et al., 2005), and 696 ± 185 neutrons $(g\ air)^{-1}$ yr^{-1} for the production rate of epithermal neutrons from fast neutrons in the atmosphere at the land/atmosphere interface (Marrero et al., 2016b). We used a high-energy

214 neutron attenuation length of 160 g cm^{-2}. The resulting ^{36}Cl age in Table 5 with its 1 σ
215 uncertainty including all analytical and production rate errors is shown with and without
216 correction for an erosion rate of 1.3 mm ka^{-1}. The ^{36}Cl age was also calculated using the
217 CRONUScalc calculator (Marrero et al., 2016a) for comparison with the results calculated
218 with the Excel® spreadsheet (Schimmelpfennig et al., 2009).

219 **4. Results**

220 *4.1. Erratics located beyond the ice marginal belt of the LLGM*

221 Exposure ages for SAAL samples show significant scatter (16.2 ± 1.4 to 115.2 ± 11.0
222 ka; Table 2). The observed variability (53.2%) is much larger than the average external
223 uncertainty (8.4%). This shows that random uncertainties are dominated by geological
224 uncertainties rather than by analytical ones. Most of the pre-LLGM exposure ages are
225 younger than 100 ka (six samples) with five ages younger than 60 ka (Table 2).

226 *4.2. Erratics of the LLGM ice marginal belt*

227 We sampled 13 erratics located on the ice marginal belt identified geomorphologically
228 as the Leszno (Brandenburg) Phase (Fig. 1B). The exposure ages for samples LGM (01 to 08)
229 and FRT (01 to 04 and 06) range between 19.3 ± 2.1 and 75.3 ± 6.3 ka (Table 2). The
230 distribution of the ages is bimodal with the narrow and high mode containing ages ranging
231 between 19.3 ± 2.1 and 25.1 ± 2.1 ka, and wider and lower mode containing ages between
232 39.5 ± 3.3 and 75.3 ± 6.3 ka (Fig. 3A). The results for the boulder that has been sampled twice
233 (LGM-02) belong to the older distribution, and are: 39.5 ± 3.3 ka for the top sample (LGM-
234 02T) and 58.6 ± 3.9 ka for the side sample (LGM-02S). The older age of the weathered side
235 of the boulder support our hypothesis that this erratic was rotated and the original top surface
236 is on the side (Fig. 2C).

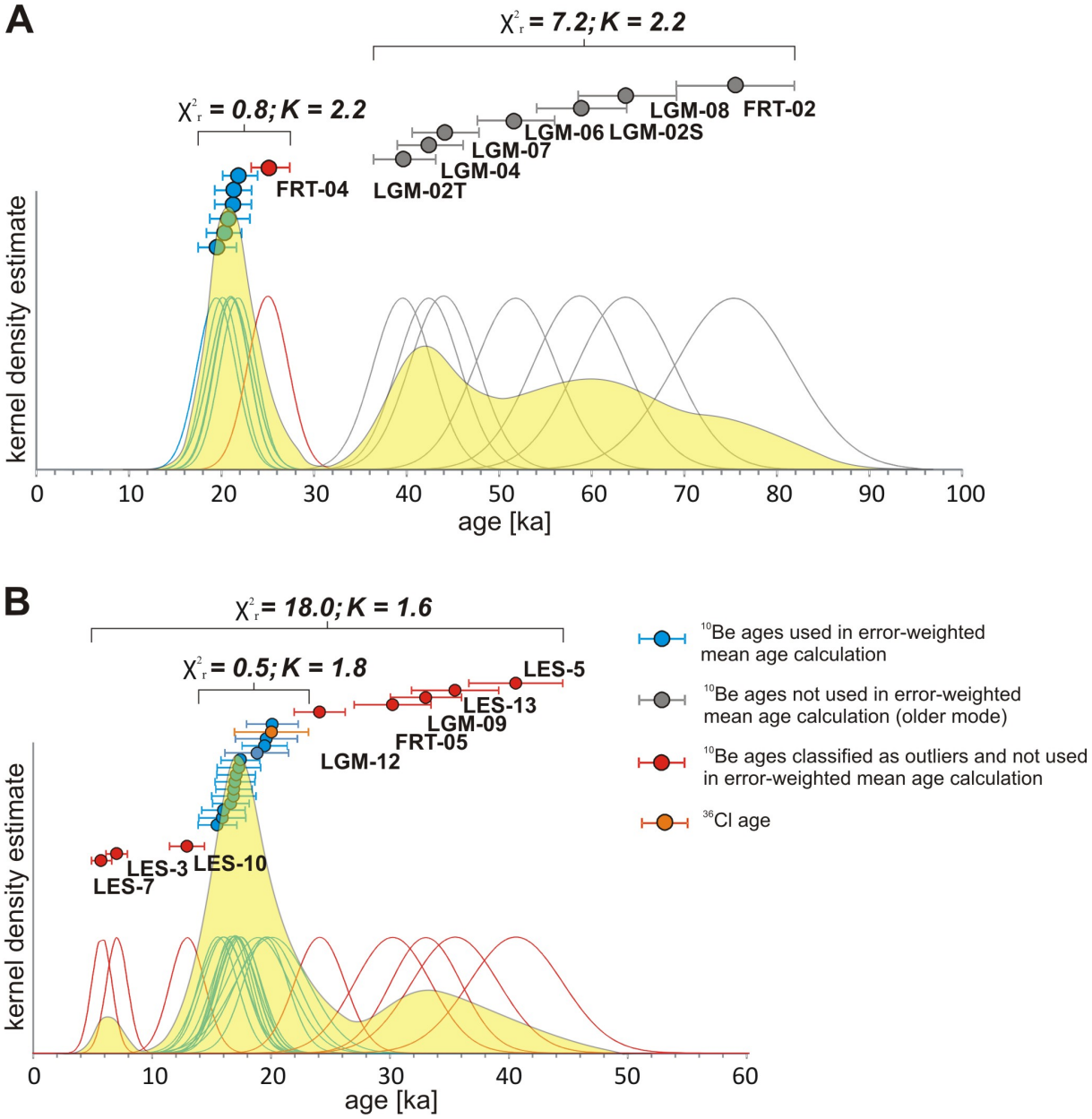

237

238 Fig. 3. Distribution of surface exposure ages for erratic boulders located on the LLGM ice
239 marginal belts. (A) Erratic ^{10}Be ages located on the ice marginal belt of the Leszno Phase. (B)
240 Surface exposure ages (22 ^{10}Be and one ^{36}Cl) of the Poznań Phase ice marginal belt. Yellow
241 areas represent cumulative kernel density estimates of all ^{10}Be ages; blue, red and grey curves
242 represent kernel density estimates for individual ^{10}Be ages: blue – included in the error-
243 weighted mean age calculation, red – outliers, grey – not accepted ages (older mode of ages
244 from ice marginal belt correlated with the Leszno Phase).

245 Ages belonging to the younger distribution are much more clustered around the mode
246 than the ages of the older distribution (Fig. 3A). The reduced chi-squared test for ages of the
247 younger distribution indicates that they represent a single population ($\chi^2_r = 0.8$ and $K = 2.2$),
248 while the ages of the older distribution do not represent a single population ($\chi^2_r = 7.2$ and $K =$
249 2.2). We used the criterion '*K*' to test whether the reduced chi-squared value fall within a 2σ
250 envelope (95% confidence). This criterion depends on the degree of freedom, and thus the
251 number of samples (n): $K = 1 + 2\sqrt{2/(n-1)}$. If $\chi^2_r < K$ then there is a >95% probability that
252 the analyzed measurements represent a single population. We therefore used the younger
253 distribution to interpret the age of the Leszno Phase ice marginal belt. The oldest age of this
254 dataset (25.1 ± 2.1 ka) was identified as an outlier according to the Chauvenet`s criterion. A
255 Shapiro-Wilk test, applied after rejecting the outlier, showed that we cannot reject the
256 normality assumption for p = 0.05 (W = 0.97) for distribution of the remaining six ages. The
257 error-weighted mean and the standard deviation of the mean calculated for these ages is 20.7
258 ± 0.8 ka (Table 2). The spatial distribution of the analyzed erratics indicates that statistically
259 reliable ages (included in the mean age calculation) are located mainly in the western part of
260 the study area (Fig. 4).
261 Twelve boulders located on the Poznań (Frankfurt) ice marginal belt were sampled for
262 ^{10}Be (samples LGM-09 to12, FRT-05, FRT-07 to 10 and FRT-12 to 14) and one boulder for
263 ^{36}Cl exposure dating (sample FRT-11). We also recalculated and used ^{10}Be ages of ten
264 boulders from published data (Rinterknecht et al., 2005, 2006), located close to the ice sheet
265 limit during the LLGM in the eastern edge of the study area (Table 2; Fig. 1B) using the same
266 procedure as for our samples.
267 ^{10}Be ages range between 5.8 ± 0.8 and 40.6 ± 3.9 ka (Table 2) with narrow modes
268 occurring at ~5–7 ka and ~15–19 ka, and wide, low mode at ~30–40 ka (Fig. 3B). The
269 youngest mode includes two ages 5.8 ± 0.8 and 7.0 ± 1.9 ka, the intermediate mode consists

of 14 ages ranging between 15.5 ± 1.6 and 20.2 ± 2.2 ka, and the oldest mode includes four ages between 30.2 ± 3.2 and 40.6 ± 3.9 ka. The reduced chi-squared test indicates that the 22 ^{10}Be ages represent multiple populations (χ^2_r = 18.0 and K = 1.6). The application of Chauvenet`s criterion identifies that the three youngest ages (<13.0 ka) and the five oldest ages (>24.1 ka) are outliers (Fig. 3B). After rejecting the outliers, the reduced chi-squared test applied to the remaining 14 ages indicates that they belong to a single population (χ^2_r = 0.5 and K = 1.8). Moreover, a Shapiro-Wilk test showed that we cannot reject the normality assumption for p = 0.05 (W = 0.90) for the distribution of the 14 ages. The error-weighted mean and the standard deviation of the error-weighted mean calculated for the ^{10}Be ages is 17.3 ± 0.5 ka (Table 2). The ^{36}Cl age is 20.1 ± 3.1 ka when calculated with the Excel® spreadsheet (Schimmelpfennig et al., 2009), and 20.0 ± 3.0 ka when calculated with the CRONUScalc calculator (Marrero et al., 2016b). These two results are very similar and belong to the same frequency distribution as the 14 ^{10}Be ages (Fig. 3B).

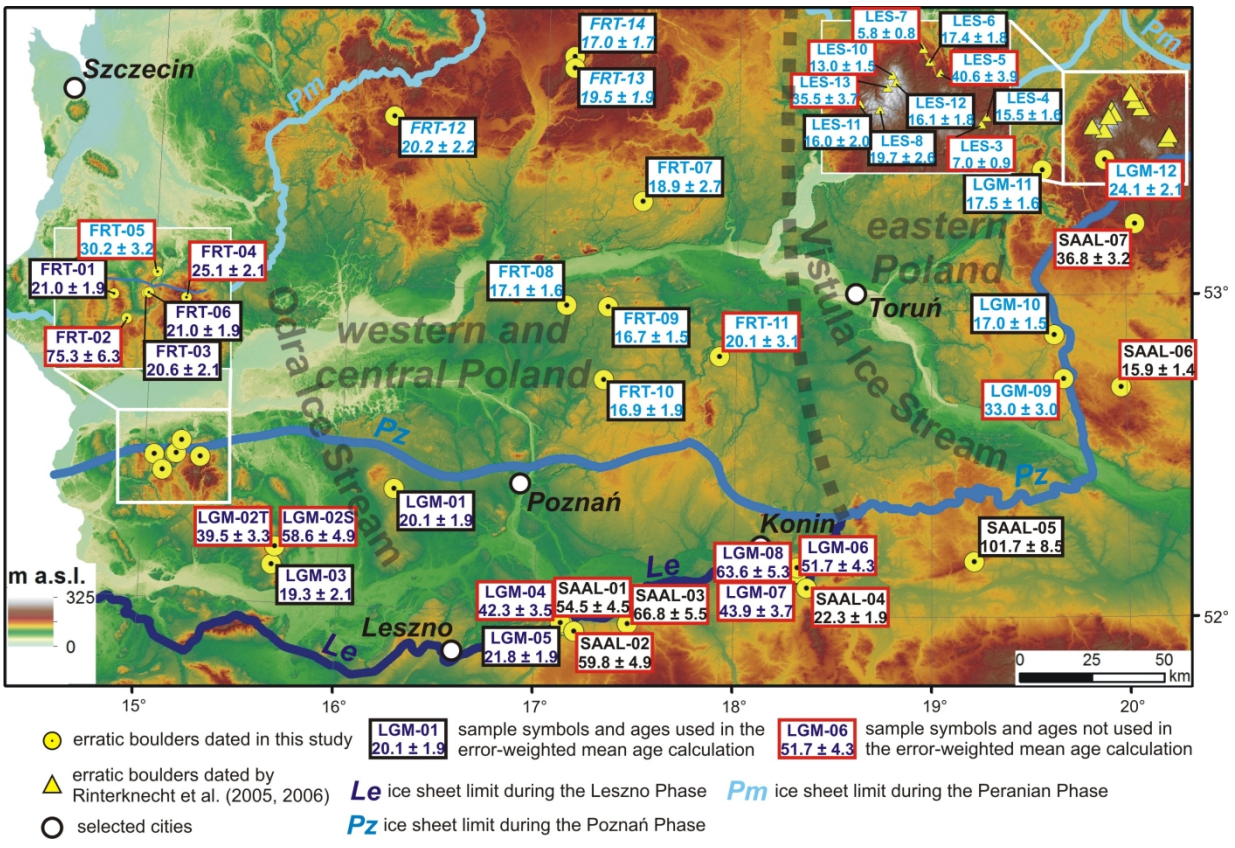

Fig. 4. Spatial distribution of ^{10}Be ages and single ^{36}Cl age in the study area. Ages used in the calculation of the error-weighted mean ages for specific ice marginal belts are framed in black frame.

5. Discussion

5.1. Pre-LLGM erratics

The distribution of the exposure ages of erratics located beyond of the ice sheet limit during the LLGM is very large (from 15.9 ± 1.4 to 101.7 ± 8.5 ka; Table 2) and these ages are not clustered around any particular time interval. We have only one exposure age (sample SAAL-05) that may be roughly interpreted as representing the timing of retreat of the MIS 6 ice sheet: 101.7 ± 8.5 ka (Table 2). Six out of seven boulders display much too young ages (from 15.9 ± 1.4 to 66.8 ± 5.5 ka) for the retreat of the MIS 6 ice sheet, and probably result from degradation of moraines and erosion of erratics (e.g. Hallet and Putkonen, 1994) during the long time period after deglaciation. Postglacial weathering and erosion of an erratic surface, removes cosmogenic nuclide accumulated in the surface layer of the sample and thus produces too young ages, but we consider the obtained exposure ages most probably represent long-term geomorphic processes acting after deglaciation, and therefore largely underestimate the timing of ice sheet retreat. Similar inconsistencies of ^{10}Be ages for erratics located within Saalian (MIS 6) landscapes were reported in Germany, in the Hocher Fläming area (Rinterknecht et al., 2012), and in Mecklenburg-Vorpommern (Rinterknecht et al., 2014) in front of the ice sheet limit during the Brandenburg Phase. For 14 erratics sampled for ^{10}Be dating in Germany, ten boulders have exposure ages too young (from 27.7 ± 1.3 to 92.8 ± 3.0 ka) for the deglaciation at the end of MIS 6 and four erratics have exposure ages ranging from 101.7 ± 10.4 to 143 ± 5.0 ka.

307 Two erratics (samples SAAL-04: 22.3 ± 1.9 ka and SAAL-06: 15.9 ± 1.4 ka) have
308 exposure ages close to the expected LLGM age, and they are also located close to the ice
309 sheet limit during the LLGM (Figs. 1 and 4). This may suggest a revision of the last SIS
310 maximum extent in central Poland. However, these erratics are located in the vicinity of the
311 sites of Eemian organic deposits that are not covered by the LLGM till (Tobolski, 1986;
312 Kuszell, 1998; Szałamacha and Skompski, 1999; Balwierz and Roman, 2002; Fig. 1). In
313 addition to geomorphology, this is a strong argument supporting that the ice sheet limit during
314 the LLGM is correct and that these two boulders display underestimated exposure ages
315 resulting from geomorphic processes.

316 *5.2. Age of the LLGM and the first stages of the last SIS retreat*

317 In central-western and northern Poland, deposition of organic sediments resting below
318 the LLGM till is dated to ~26.5–25.2 cal ka BP (Table 1) indicating that the maximum extent
319 of the last SIS in this region occurred later than ~25 cal ka BP. Moreover, the radiocarbon age
320 of the basal part of gyttja (21.4 ± 1.9 cal ka BP) resting on the same till (Stankowski et al.,
321 1999) indicates that the ice sheet retreat from its maximum limit started not earlier than ~21.4
322 cal ka BP. Recently, Marks (2012) determined, based on his interpretation of the available
323 ages, the age of the maximum extent of the last SIS in central and western Poland during the
324 Leszno Phase at 24 cal ka BP.

325 Our results for the Leszno (Brandenburg) Phase in western Poland are clustered
326 around two modes at ~19–22 ka and ~40–70 ka (Fig. 3A). We used this younger mode to
327 calculate an error-weighted mean surface exposure age of 20.7 ± 0.8 ka (Fig. 5). We interpret
328 this age as a minimum age of the commencement of the ice sheet retreat from its maximum
329 limit at the end of the LLGM in central and western Poland. Ages used in the error-weighted
330 mean age calculation agree, within uncertainty, with the radiocarbon ages coming from
331 deposits resting below and above the till of the ice advance during the Leszno Phase in central

Poland (Stankowski et al., 1999). The ages of the older distribution (between 39.5 ± 3.3 and 75.3 ± 6.3 ka) probably result from inherited ^{10}Be. This could have happened either due to redeposition of previously exposed boulders by the last SIS with no or limited erosion (cf. Håkansson et al., 2008; Rinterknecht et al., 2012).

The new exposure age of the last ice sheet retreat in western Poland is also consistent with most luminescence ages constraining the timing of the Leszno Phase (Fig. 5). OSL dating of fluvial, fluvioglacial and periglacial sediments underlying the till correlated with the Leszno Phase (Stankowski et al., 1999; Wysota et al., 2009; Molewski and Weckwerth, 2009; Weckwerth et al., 2011) yields ages that mostly range between ~29 and ~24 ka. Additionally, OSL ages of sediments underlying the LLGM till in the northernmost region of Germany suggest that the last ice sheet reached the southern Baltic coast at Rügen Island after 22.7 ± 1.9 ka (Pisarska-Jamroży et al., 2018) or 22.0 ± 2.0 ka and 23.0 ± 2.0 ka (Kenzler et al., 2015, 2017). OSL ages of fluvial and periglacial deposits overlying the till correlated with the Leszno Phase in Poland range between ~21 and 19 ka (Molewski 2007; Wysota et al., 2009; see Fig. 5). We thus suggest that the error-weighted mean exposure age of erratics in western Poland (20.7 ± 0.8 ka) represents the most reliable age for the initiation of the ice sheet retreat after the ice advance during the Leszno Phase.

Our results also corroborate TCN data published by Heine et al. (2009), who determined the exposure ^{10}Be age of three boulders located on the Brandenburg (Leszno) and Frankfurt (Poznań) Phase ice marginal belts in north-eastern Germany. Our error-weighted mean exposure age (20.7 ± 0.8 ka) and the results of Heine et al. (2009) (22.0 ± 1.1 ka), are coeval within uncertainties. We suggest that the duration of the LLGM in central and western Poland, constrained with the available radiocarbon ages and our new ^{10}Be exposure ages, is between ~25 ka and ~21 ka (Fig. 5).

Radiocarbon dating from western Belarus (Zimenkov, 1989) indicates an age of the last SIS maximum extent of ~22.5 cal ka BP in the eastern part of its southern sector. The deglaciation of this region, in the light of radiocarbon dating in north-eastern Poland (Gamrat et al., 2017), started not earlier than 19.1 ± 0.2 cal ka BP. Our results for erratics located close to the ice sheet limit during the LLGM in the eastern part of the study area also support this view (Fig. 5). TCN exposure ages of boulders located on the ice marginal belt of the Poznań Phase, after rejecting outliers with Chauvenet`s criterion, range between 15.5 ± 1.6 and 20.2 ± 2.2 ka, with an average age of 17.3 ± 0.5 ka (Table 2). We interpret these ages as a minimum age of:

1) the beginning of the ice sheet retreat during the LLGM in eastern Poland, after the ice advance during the Poznań Phase,
2) the ice sheet retreat from the Poznań Phase limit in north-central Poland, postdating the LLGM represented by the Leszno Phase.

These results are in general agreement with OSL ages (~18.7–16.7 ka; Fig. 5) of fluvioglacial sand overlying the till correlated with the ice advance during the Poznań Phase in north-central Poland (Stankowski et al., 1999; Wysota et al., 2009; Roman, 2017). ^{10}Be exposure dating of erratics located on moraines correlated with the LLGM in Belarus and Lithuania (Rinterknecht et al., 2007, 2008) yields mean exposure ages of deglaciation at 17.7 ± 0.8 and 20.1 ± 1.2 ka respectively. Furthermore, the recent results from Valday Heights in NW Russia show a ^{10}Be age for the LLGM at 18.9 ± 0.5 ka (Rinterknecht et al., 2018). These data suggest an older age for the LLGM further east of eastern Poland. We propose a possible duration for the LLGM in eastern Poland, constrained by radiocarbon ages and our new ^{10}Be exposure ages as well as recalculated data of Rinterknecht et al. (2005, 2006), between ~22 ka and ~18 ka (Fig. 5).

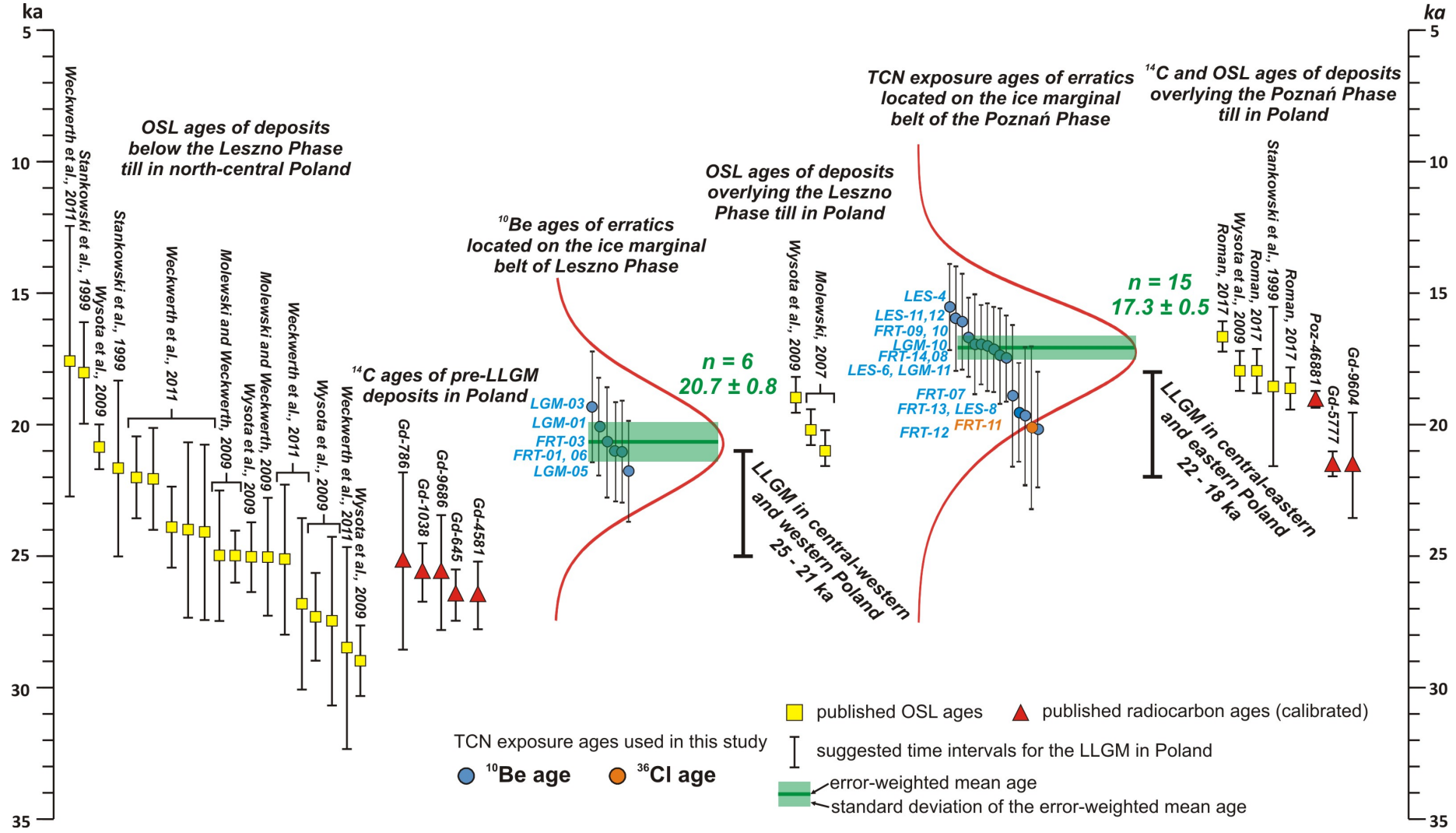

Fig. 5. Distribution of TCN, ^{14}C, and OSL ages relevant for the reconstruction of the timing of the LLGM and the initiation of the last ice sheet retreat in the study area. Sources of ^{14}C ages are listed in Table 1.

383 Our results do not agree with OSL data and reinterpretation of ^{10}Be exposure dating of
384 erratics proposed recently by Hardt et al. (2016). Based on OSL dating of fluvioglacial
385 deposits in the vicinity of the Frankfurt (Poznań) ice marginal belts, they assigned the age of
386 ~26.3 ± 3.7 ka for the initiation of the ice sheet retreat in north-eastern Germany. This is
387 significantly older than our mean exposure age of 17.3 ± 0.5 ka, which we interpret as a
388 minimum age of the start of deglaciation during the Poznań Phase in northern Poland. The
389 inconsistency may result from the overestimation of the OSL ages obtained by Hardt et al.
390 (2016), due to incomplete bleaching of fluvioglacial sediments. Although these authors
391 applied a single grain method and minimum age model in OSL age calculation, the risk that
392 all quartz grains within the sample are not fully bleached persists, especially when
393 fluvioglacial (outwash) sediments deposited close to the ice margin are dated (e.g. Houmark-
394 Nielsen, 2008; Bickel et al., 2015). However, if the OSL ages were correct for the ice sheet
395 recession, it would suggest a high asynchrony of the ice margin retreat during the Poznań
396 (Frankfurt) Phase: the beginning of the ice sheet retreat in northern Poland occurred at least
397 ~5 ka later than in north-eastern Germany. Furthermore, Hardt et al. (2016) interpreted the
398 recalculated surface exposure ages of Heine et al. (2009) as an indicator of landform
399 stabilization after deglaciation rather than a reliable age of the ice-sheet retreat (Houmark-
400 Nielsen et al., 2012). On the other hand, our exposure ages of erratics in the study area
401 correlate strongly with independent geochronological data from Poland, such as OSL dating,
402 and we argue that they represent a reliable age for the initiation of the ice sheet retreat in the
403 study area. They also correlate with the OSL ages cited above and recently obtained on Rügen
404 Island (Kenzler et al., 2015, 2017; Pisarska-Jamroży et al., 2018).

405 *5.3. Asynchrony of LLGM*

406 Although already postulated by other authors (e.g. Marks 2012; Larsen et al., 2016;
407 Stroeven et al., 2016; Patton et al., 2017) the asynchrony of the LLGM ice sheet limit in the

southern sector of the SIS was strongly confirmed by our results. TCN dating of the ice front retreat along the last SIS ice margin in northern Poland show clearly a ~3 ka delay of the LLGM in the eastern Poland with respect to the LLGM in western and central Poland. This generally agrees with the recent reconstructions of the diachronous LLGM dated at ~24 ka (Leszno/Brandenburg Phase) in the western part and at ~19 ka (Poznań/Frankfurt Phase) in the eastern part of the study area (Wysota et al., 2009; Marks, 2011, 2012, 2015). This asynchrony of the LLGM may be related to the activation and deactivation of the Vistula and Odra ice streams (Wysota et al., 2009; Woźniak and Czubla, 2015; Spagnolo et al., 2016; Roman, 2017). These ice streams most likely shaped the ice margin (Fig. 5) and to a large extent controlled the timing of the last SIS retreat.

Timing of the ice margin retreat within the last SIS have been recently reconstructed based on GIS compilation of available geochronological data and construction of the deglaciation isochrones (Hughes et al., 2016, Stroeven et al., 2016). The reconstruction for the Eurasian ice sheets suggests the maximum ice sheet extent within the southern sector of the last SIS 24–22 ka, with the LLGM in western Poland most likely 24–23 ka and the LLGM in eastern Poland most likely 22 ka (Hughes et al., 2016). Our results of TCN dating indicate larger time offset between the maximum ice sheet expansion in western and eastern Poland. They correspond more closely to the reconstruction of Stroeven et al. (2016), who interpreted the timing of the LLGM to be 22 ka in western and 19 ka in eastern Poland.

6. Conclusions

1. A wide distribution of erratic exposure ages located on the pre-LLGM moraine plateaux (15.9 ± 1.4 to 101.7 ± 8.5 ka) is not clustered around any particular time interval. The ^{10}Be exposure ages represent long-term postglacial geomorphic processes.

2. ^{10}Be exposure dating of erratics resting on the ice marginal belt of the Leszno (Brandenburg) Phase in western Poland show the initiation of the ice sheet retreat 20.7 ± 0.8 ka.

3. The duration of the LLGM in western and central Poland, constrained by our ^{10}Be exposure dating and the available radiocarbon dating is between ~25 ka and ~21 ka.

4. ^{10}Be exposure dating of erratics resting on the ice marginal belt of the Poznań Phase show the initiation of the last SIS retreat 17.3 ± 0.5 ka.

5. The duration of the LLGM in eastern Poland is best constrained by our new ^{10}Be exposure ages, recalculated exposure ages of Rinterknecht et al. (2005, 2006) and calibrated radiocarbon ages is between ~22 ka and ~18 ka.

6. Our results confirm that different sectors of the last SIS southern front advanced and retreated asynchronously. The LLGM ice limit in western and central Poland is probably ~3 ka older than in eastern Poland. The documented asynchrony supports a complex response of the last SIS southern margin to hemispheric climatic fluctuations and internal dynamics of the ice sheet controlled largely by activation and deactivation of ice streams.

Acknowledgements

We are very grateful to the Regional Directorates of Environmental Protection local communes offices for permissions for sampling large erratics protected by law. We appreciate suggestions of two anonymous reviews and of the editor which help to improve the manuscript.

Research is funded by: National Science Centre grant no. 2014/15/D/ST10/04113 to Karol Tylmann. The ASTER AMS national facility (CEREGE, Aix en Provence) is supported by

455 the INSU/CNRS, the ANR through the "Projets thématiques d’excellence" program for the
456 "Equipements d’excellence" ASTER-CEREGE action and IRD.

457 **7. References**

458 1. Arnold, M., Merchel, S., Bourlés, D.L., Braucher, R., Benedetti, L., Finkel, R.C.,
459 Auma□tre, G., Gottdang, A., Klein, M., 2010. The French accelerator mass
460 spectrometry facility ASTER: Improved performance and developments. Nuclear
461 Instruments and Methods in Physics Research B 268, 1954–1959.

462 2. Balco, G., Stone, J.O., Lifton, N.A., Dunai, T.J., 2008. A complete and easily
463 accessible means of calculating surface exposure ages or erosion rates from ^{10}Be and
464 ^{26}Al measurements. Quaternary Geochronology 3, 174–195.

465 3. Balwierz, Z., Roman, M., 2002. A new Eemian Interglacial to Early Vistulian site at
466 Łanięta, central Poland. Geological Quarterly 46, 207–217.

467 4. Bickel, L., Lüthgens, C., Lomax, J., Fiebig, M., 2015. Luminescence dating of
468 glaciofluvial deposits linked to the penultimate glaciation in the Eastern Alps
469 Quaternary International 357, 110–124.

470 5. Bitinas, A., 2012. New sights into the last deglaciation of the southeastern flank of the
471 Scandinavian Ice Sheet. Quaternary Science Reviews 44, 69–80.

472 6. Borchers, B., Marrero, S., Balco, G., Caffee, M., Goehring, B., Lifton, N., Nishiizumi,
473 K., Philips, F., Schaefer, J., Stone, J., 2016. Geological calibration of spallation
474 production rates in the CRONUS-Earth project. Quaternary Geochronology 31, 188–
475 198.

476 7. Braucher, R., Guillou, V., Bourlès, D. L., Arnold, M., Aumaître, G., Keddadouche, K.,
477 Nottoli, E., 2015. Preparation of ASTER in-house $^{10}Be/^{9}Be$ standard solutions.
478 Nuclear Instruments and Methods in Physics Research B 361, 335–340.

479 8. Chmeleff, J., von Blanckenburg, F., Kossert, K., Jakob, D., 2010. Determination of the
480 ^{10}Be half-life by multicollector ICP-MS and liquid scintillation counting. Nuclear
481 Instruments and Methods in Physics Research Section B: Beam Interactions with
482 Materials and Atoms 268, 192–199.

483 9. Clark, P.U., Dyke, A.S., Shakun, J.D., Carlson, A.E., Clark, J., Wohlfarth, B.,
484 Mitrovica, J.X., Hostetler, S.W., McCabe, A.M., 2009. The Last Glacial Maximum.
485 Science 325, 710–714.

486 10. Fink, D., Vogt, S., Hotchkis, M., 2000. Cross-sections for ^{36}Cl from Ti at Ep=35–150
487 MeV: Applications to in-situ exposure dating. Nuclear Instruments and Methods in
488 Physics Research Section B: Beam Interactions with Materials and Atoms 172, 861–
489 866.

490 11. Galon, R., Roszkówna, L., 1961. Extents of the Scandinavian glaciations and of their
491 recession stages on the territory of Poland in the light of analysis of the marginal
492 forms of inland ice. Przegląd Geograficzny 33, 347–364.

493 12. Gamrat, W.W., Błaszkiewicz, M., Andrzejewski, L., Krześlak, I., 2017.
494 Asynchronous development of two Late Glacial lake basins near the Drwęca ice-
495 marginal valley (N Poland). Geological Quarterly 61, 450–464.

496 13. Gogołek, W., Mańkowska, A. 1989. Vistulian of the Turek Upland in the light of new
497 data. Kwartalnik Geologiczny 33, 573–586.

14. Gosse, J.C., Evenson, E.B., Klein, J., Lawn, B., Middleton, R., 1995. Precise cosmogenic ^{10}Be measurements in western North America: support for a global Younger Dryas cooling event. Geology 23, 877–880.

15. Hallet, B., Putkonen, J., 1994. Surface exposure dating of dynamic landforms: young boulders on aging moraines. Science 265, 937–940.

16. Hardt, J., Lüthgens, C., Hebenstreit, R., Böse, M., 2016. Geochronological (OSL) and geomorphological investigations at the presumed Frankfurt ice marginal position in northeast Germany. Quaternary Science Reviews 154, 85–99.

17. Håkansson, L., Alexanderson, H., Hjort, C.,Möller, P., Briner, J.P., Aldahan, A., Possnert, G., 2008. Late Pleistocene glacial history of Jameson land, central east Greenland, derived from cosmogenic ^{10}Be and ^{26}Al exposure dating. Boreas 38, 244–260.

18. Heine, K., Reuther, A.U., Thieke, H.U., Schulz, R., Schlaak, N., Kubik, P.W., 2009. Timing of Weichselian ice marginal positions in Brandenburg (northeastern Germany) using cosmogenic in situ ^{10}Be. Zeitschrift für Geomorphologie NF 53, 433–454.

19. Houmark-Nielsen, M., 2008. Testing OSL failures against a regional Weichselian glaciations chronology from southern Scandinavia. Boreas 37, 660–677.

20. Houmark-Nielsen, M., Kjaer, K.H., 2003. Southwest Scandinavia, 40–15 kyr BP: palaeogeography and environmental change. Journal of Quaternary Science 18, 769–786.

21. Houmark-Nielsen, M., Linge, H., Fabel, D., Schnabel, C., Xu, S., Wilcken, K.M., Binnie, S., 2012. Cosmogenic surface exposure dating the last deglaciation in

520 Denmark: Discrepancies with independent age constraints suggest delayed periglacial
521 landform stabilisation. Quaternary Geochronology 13, 1–17.

522 22. Hughes, A.L.C., Gyllencreutz, R., Lohne, Ø.S., Mangerud, J., Svendsen, J.I., 2016.
523 The last Eurasian ice sheets e a chronological database and time-slice reconstruction,
524 DATED-1. Boreas 45, 1–45.

525 23. Hughes, P.D., Gibbard, P.L., 2015. A stratigraphical basis for the Last Glacial
526 Maximum (LGM). Quaternary International 383, 174–15.

527 24. Hughes, P.D., Gibbard, P.L., Ehlers, J., 2013. Timing of glaciation during the last
528 glacial cycle: evaluating the concept of a global 'Last Glacial Maximum' (LGM).
529 Earth Science Reviews 125, 171–198.

530 25. Kasprzak, L., 1988. Differentiation mechanism in the formation of marginal zones of
531 Leszno and Poznań Phases of the Last Glaciation, Great Poland Lowland.
532 Dokumentacja Geograficzna 5–6, 159 pp (in Polish with English summary).

533 26. Kenzler, M., Tsukamoto, S., Meng, S., Frechen, M., Hüneke, H., 2017. New age
534 constraints from the SW Baltic Sea area – implications for Scandinavian Ice Sheet
535 dynamics and palaeo-environmental conditions during MIS 3 and early MIS 2. Boreas
536 46, 34–52.

537 27. Kenzler, M., Tsukamoto, S., Meng, S., Thiel, C., Frechen, M., Hüneke, H., 2015.
538 Luminescence dating of Weichselian interstadial sediments from the German Baltic
539 Sea coast. Quaternary Geochronology 30, 215–256.

540 28. Korschinek, G., Bergmaier, A., Faestermann, T., Gerstmann, U.C., Knie, K., Rugel,
541 G., Wallner, A., Dillmann, I., Dollinger, G., von Gostomski, C.L., 2010. A new value

542 for the half-life of ^{10}Be by Heavy-Ion Elastic Recoil Detection and liquid scintillation
543 counting. Nuclear Instruments and Methods in Physics Research Section B: Beam
544 Interactions with Materials and Atoms 268, 187–191.

545 29. Kozarski, S., 1988. Time and dynamics of the last Scandinavian ice-sheet retreat from
546 northwestern Poland. Geographia Polonica 55, 91–101.

547 30. Kozarski, S., 1995. Deglaciation of northwestern Poland: environmental conditions
548 and geosystem transformation ~20 ka → 10 ka BP. Dokumentacja Geograficzna 1, 82
549 pp. (in Polish).

550 31. Kramarska, R., 1998. Origin and development of the Odra bank in the light of the
551 geologic structure and radiocarbon dating. Geological Quarterly 42, 277–288.

552 32. Krzyszkowski, D., Dobracka, E., Dobracki, R., Czerwonka, J., Kuszell, T., 1999.
553 Stratigraphy of Weichselian deposits in the cliff sections between Łukęcin and
554 Niechorze, Baltic coast, Northwestern Poland. Quaternary Studies in Poland 16, 27–
555 45.

556 33. Kuszell, T., 1998. New sites of the interglacial deposits in south-western Poland.
557 Biuletyn Państwowego Instytutu Geologicznego 385, 127–142 (in Polish).

558 34. Lal, D., 1991. Cosmic ray labeling of erosion surfaces: In situ nuclide production rates
559 and erosion models. Earth Planetary Science Letters 104, 424–439.

560 35. Larsen, E., Fredin, O., Lysså, A., Amantov, A., Fjeldskaar, W., Ottesen, D., 2016.
561 Causes of time-transgressive glacial maxima positions of the last Scandinavian Ice
562 Sheet. Norwegian Journal of Geology 96, 159–170.

563 36. Lasberg, K., Kalm, V., 2013. Chronology of Late Weichselian glaciation in the
564 western part of the East European Plain. Boreas 42, 995–1007.

565 37. Lüthgens, C., Böse, M., Preusser, F., 2011. Age of the Pomeranian ice-marginal
566 position in northeastern Germany determined by Optically Stimulated Luminescence
567 (OSL) dating of glaciofluvial sediments. Boreas 40, 598–615.

568 38. Majdanowski, S., 1947. Rozmieszczenie, gęstość i kierunki rynien jeziornych na Niżu
569 Polskim. Przegląd Geograficzny 21, 37–69.

570 39. Marks, L., 2002. Last Glacial Maximum in Poland. Quaternary Science Reviews 21,
571 103–110.

572 40. Marks, L., 2011. Quaternary glaciations in Poland. In: Ehlers, J., Gibbard, P.L.,
573 Hughes, P.D. (eds.), Quaternary Glaciations – Extent and Chronology: A Closer Look.
574 Developments in Quaternary Science, 15. Elsevier, Amsterdam, pp. 299–304.

575 41. Marks, L., 2012. Timing of the Late Vistulian (Weichselian) glacial phases in Poland.
576 Quaternary Science Reviews 44, 81–88.

577 42. Marks, L., 2015. Last deglaciation of northern continental Europe. Cuadernos de
578 Investigación Geográfica 41(2), 279–293.

579 43. Marks, L., Ber A., Gogołek W., Piotrowska, K. (eds.), 2006. Mapa Geologiczna Polski
580 1:500 000. Ministerstwo Środowiska, PIG-PIB, Warszawa.

581 44. Marrero, S.M., Philips, F.M., Borchers, B., Lifton, N., Aumer, R., Balco, G., 2016a.
582 Cosmogenic nuclide systematics and the CRONUScalc program. Quaternary
583 Geochronology 31, 160–187.

584 45. Marrero, S.M., Phillips, F.M., Caffee, M.W., Gosse, J.C., 2016b. CRONUS-Earth
585 cosmogenic ^{36}Cl calibration. Quaternary Geochronology 31, 199–219.

586 46. Mix, A.C., Bard, E., Schneider, R., 2001. Environmental processes of the ice age:
587 land, oceans, glaciers (EPILOG). Quaternary Science Reviews 20, 627–657.

588 47. Molewski P, 2007. Neotectonic and glaciodynamic conditions for the formation of the
589 Pleistocene of the Kujawy Moraine Plateau). Wydawnictwo Naukowe Uniwersytetu
590 Mikołaja Kopernika, Toruń, 140 pp. (in Polish).

591 48. Molewski, P., Weckwerth, P., 2009. Explanatory text to the Detailed geological map
592 of Poland in the scale 1 : 50 000, ark. Toruń. Centr. Arch. Geol. PIG-PIB, Warszawa
593 (in Polish).

594 49. Narloch, W., Wysota, W., Piotrowski, J.A., 2013. Sedimentological record of
595 subglacial conditions and ice sheet dynamics of the Vistula Ice Stream (north-central
596 Poland) during the Last Glaciation. Sedimentary Geology 293, 30–44.

597 50. Niewiarowski, W., 1995. Fluctuations of the water level in the Biskupin lake and their
598 reasons. In: Niewiarowski W. (ed.) Outline of geographical environment`s changes
599 under the influence of natural and anthropogenic factors in Late Glacial and Holocene:
600 215–234. Wydawnictwo Turpress, Toruń (in Polish).

601 51. Patton, H., Hubbard, A., Andreassen, K., Auriac, A., Whitehouse, P.L, Stroeven, A.P.,
602 Shackleton, C., Winsborrow, M., Heyman, J., Hall, A.M., 2017. Deglaciation of the
603 Eurasian ice sheet complex. Quaternary Science Reviews 169, 148–172.

604 52. Pisarska-Jamroży, M., Bełżyt, Sz., Börner, A., Hoffmann, G., Hüneke, H., Kenzler M.,
605 Obst, K., Rother, H., van Loon, A.J. (Tom), 2018. Evidence from seismites for glacio-

606 isostatically induced crustal faulting in front of an advancing land-ice mass (Rügen
607 Island, SW Baltic Sea). Tectonophysics 745, 338–348.

608 53. Plug, L.J., Gosse, J.C., McIntosh, J.J., Bigley, R., 2007. Attenuation of cosmic ray flux
609 in temperate forests. Journal of Geophysical Research 112,
610 http://dx.doi.org/10.1029/2006JF000668.

611 54. Reimer, P.J., Bard, E., Bayliss, A., Beck, J.W., Blackwell, P.G., Ramsey, C.B., Buck,
612 C.E., Cheng, H., Edwards, R.L., Friedrich, M., Grootes, P.M., Guilderson, T.P.,
613 Haflidason, H., Hajdas, I., Hatté, C., Heaton, T.J., Hoffmann, D.L., Hogg, A.G.,
614 Hughen, K.A., Kaiser, K.F., Kromer, B., Manning, S.W., Niu, M., Reimer, R.W.,
615 Richards, D.A., Scott, E.M., Southon, J.R., Staff, R.A., Turney, C.S.M., van der Plicht,
616 J., 2013. INTCAL13 AND MARINE13 radiocarbon age calibration curves 0-50,000
617 years cal BP. Radiocarbon 55, 1869–1887.

618 55. Rinterknecht V.R., Bitinas, A., Clark, P.U., Raisbeck, G.M., Yiou, F. & Brook, E.J.,
619 2008, Timing of the last deglaciation in Lithuania, Boreas 37, 426–433.

620 56. Rinterknecht, V.R., Börner, A., Bourlès, D., Braucher, R., 2014. Cosmogenic ^{10}Be
621 dating of ice sheet marginal belts in Mecklenburg-Vorpommern, Western Pomerania
622 (northeast Germany). Quaternary Geochronology 19, 42–51.

623 57. Rinterknecht, V., Braucher, R., Böse, M., Bourlès, D., Mercier, J.L., 2012. Late
624 Quaternary ice sheet extents in northeastern Germany inferred from surface exposure
625 dating. Quaternary Science Reviews 44, 89–95.

626 58. Rinterknecht, V.R., Marks, L., Piotrowski, J.A., Raisbeck, G.M., Yiou, F., Brook, E.J.,
627 Clark, P.U., 2005. Cosmogenic ^{10}Be ages on the Pomeranian moraine, Poland. Boreas
628 34, 186–191.

629 59. Rinterknecht, V.R., Clark, P.U., Raisbeck, G.M.,Yiou, F., Bitinas, A., Brook, E.J.,
630 Marks, L., Zelčs, V., Lunkka, J.-P., Pavlovskaya, I.E., Piotrowski, J.A., Raukas, A.,
631 2006. The last deglaciation of the southeastern sector of the Scandinavian ice sheet.
632 Science 311, 1449–1452.

633 60. Rinterknecht, V., Hang, T., Gorlach, A., Kohv M., Kalla, K., Kalm, V., Subetto, D.,
634 Bourlès, D., Léanni, L., Guillou, V., ASTER Team, 2018. The Last Glacial Maximum
635 extent of the Scandinavian Ice Sheet in the Valday Heights, western Russia: Evidence
636 from cosmogenic surface exposure dating using ^{10}Be. Quaternary Science Reviews
637 200, 106–113.

638 61. Rinterknecht V.R., I.E. Pavlovskaya, P.U. Clark, G.M. Raisbeck, F. Yiou, E.J. Brook,
639 2007, Timing of the Last Deglaciation in Belarus, Boreas 36, 307–313.

640 62. Roman, M., 2017. Ice-flow directions of the last Scandinavian Ice Sheet in central
641 Poland, Quaternary International, https://doi.org/10.1016/j.quaint.2017.11.035.

642 63. Rotnicki, K., Borówka, R.K., 1995. The Last Cold Period in the Gardno-Łeba Coastal
643 Plain. Journal of Coastal Research 22, 225–229.

644 64. Schimmelpfennig, I., Benedetti, L., Finkel, R., Pik, R., Blard, P.H., Bourlès, D.,
645 Burnard, P., Williams, A., 2009. Sources of in-situ ^{36}Cl in basaltic rocks. Implications
646 for calibration of production rates. Quaternary Geochronology 4, 441–461.

647 65. Schimmelpfennig, I., Benedetti, L., Garreta, V., Pik, R., Blard, P.H., Burnard, P.,
648 Bourlès, D., Finkel, R., Ammon, K., Dunai, T., 2011. Calibration of cosmogenic ^{36}Cl
649 production rates from Ca and K spallation in lava flows from Mt. Etna (38°N, Italy)
650 and Payun Matru (36°S, Argentina). Geochimica Cosmochimica Acta 75, 2611–2632.

651 66. Schimmelpfennig, I., Schaefer, J.M., Putnam, A.E., Koffman, T., Benedetti, L., Ivy-
652 Ochs, S., Team, A., Schlüchter, C., 2014. ^{36}Cl production rate from K-spallation in the
653 European Alps (Chironico landslide, Switzerland). Journal of Quaternary Science 29,
654 407–413.

655 67. Spagnolo, M., Philips, E., Piotrowski, J.A., Rea, B.R., Clark, C.D., Stokes, C.R., Carr,
656 S.J., Ely, J.C., Ribolini, A., Wysota, W., Szuman, I., 2016. Ice stream motion
657 facilitated by a shallow-deforming and accreting bed. Nature Communications 7,
658 10723, doi:10.1038/ncomms10723.

659 68. Stankowska, A., Stankowski, W., 1988. Maximum extent of the Vistulian ice sheet in
660 the vicinity of Konin, Poland: a geomorphological, sedimentological and radiometric
661 evidence. Geographia Polonica 55, 141–150.

662 69. Stankowski, W., Bluszcz, A., Nita, M., 1999. Upper Quaternary deposits sites
663 Mikorzyn and Sławoszewek in the light of geological investigation, radiocarbon and
664 thermoluminescence dating, and palynological analysis. In: Pazur, A., Bluszcz, A.,
665 Stankowski, W., Starkel, L. (eds.), Geochronology of Upper Quaternary of Poland in
666 the light of radiocarbon and luminescence dating. Institute of Physics Silesian
667 University of Technology Press, Gliwice, 87–111 (in Polish).

668 70. Stone, J., 2000. Air pressure and cosmogenic isotope production. Journal of
669 Geophysical Research 105, 23753–23760.

670 71. Stone, J.O., Fifielde, K., Vasconcelos, P., 2005. Terrestrial chlorine-36 production
671 from spallation of iron, in: Abstract of 10th International Conference on Accelerator
672 Mass Spectrometry. Berkeley, CA.

673 72. Stroeven, A.P., Hättestrand, C., Kleman, J., Heyman, J., Fabel, D., Fredin, O.,
674 Goodfellow, B.W., Harbor, J.M., Jansen, J.D., Olsen, L., Caffee, M.W., Fink, D.,
675 Lundqvist, J., Rosqvist, G.C., Strömberg, B., Jansson, K.N., 2016. Deglaciation of
676 Fennoscandia. Quaternary Science Reviews 147, 91–121.

677 73. Stroeven, A.P., Heyman, J., Fabel, D., Björck, S., Caffee, M.W., Fredin, O., Harbore,
678 J.M. 2015. A new Scandinavian reference ^{10}Be production rate. Quaternary
679 Geochronology 29, 104–115.

680 74. Stuiver, M., Reimer, P.J., Reimer, R.W., 2017. CALIB 7.1 [WWW program] at
681 http://calib.org, accessed 2017-1-19.

682 75. Szałamacha, G., Skompski, S., 1999. Biogenic sediments of the Eemian Interglacial at
683 Krzyżówki near Koło, central Poland. Geological Quarterly 43, 99–106.

684 76. Tobolski, K., 1986. Paleobotanical studies of the Eemian interglacial and early
685 Vistulian, Władysławów in the vicinity of Turek (preliminary report). Quaternary
686 Studies in Poland 7, 1–101.

687 77. Tylmann, K., Woźniak, P.P., Rinterknecht V., 2018. Erratics selection for cosmogenic
688 nuclide exposure dating – an optimization approach. Baltica 31(2), 100–114.

689 78. Weckwerth, P., Przegiętka, K., Chruścińska, A., Woronko, B., Oczkowski, H.L., 2011.
690 Age and sedimentological features of fluvial series in the Toruń basin and the Drwęca
691 valley (Poland). Geochronometria 38, 397–412.

692 79. Woźniak, P.P., Czubla P., 2015. The Late Weichselian glacial record in northern
693 Poland – towards a wider perspective: a new look at debris transport routes by the FIS.
694 Quaternary International 386, 3–17.

80. Wysota, W., Molewski, P., Sokołowski, R.J., 2009. Record of the Vistula ice lobe advances in the Late Weichselian glacial sequence in north-central Poland. Quaternary International 207, 26–41.

81. Zimenkov, O., 1989. Age of the maximum extent of the Poozerian Glaciation in Belarus. New data about Cenozoic geology of Belarus and adjacent areas. In. Matveyev, A. (ed.) Nauka i tekhnika, 30–44, Minsk, Belarus (in Russian).

Table 1. Published radiocarbon ages significant for the timing of the last SIS advance and retreat along the LLGM limit in Poland.

Laboratory symbol	^{14}C age (ka BP)	Calibrated age (cal ka BP)*	Dated material	Locality	Reference
Post-LLGM ages					
Poz-46881	15.9 ± 0.1	19.1 ± 0.2	dispersed organic matter in laminated lacustrine silt	Piotrowo (Poland)	Gamrat et al. (2017)
Gd-5777	17.7 ± 0.2	21.4 ± 0.6	dispersed organic matter in lacustrine silt	Biskupińskie Lake (Poland)	Niewiarowski (1995)
Gd-9604	17.7 ± 0.8	21.4 ± 1.9	peat at the bottom of gyttja	Sławoszewek (Poland)	Stankowski et al. (1999)
Pre-LLGM ages					
Gd-786	21.2 ± 1.6	25.2 ± 3.4	dispersed organic matter in silt below till	Żdzary (Poland)	Gogołek and Mańkowska (1989)
Gd-1038	21.5 ± 0.4	25.6 ± 1.1	dispersed organic matter in silt below till	Odra Bank (Poland)	Kramarska (1998)
Gd-9686	21.6 ± 1.1	25.6 ± 2.2	organic matter below till	Niechorze (Poland)	Krzyszkowski et al. (1999)
Gd-645	22.1 ± 0.5	26.4 ± 0.9	peat below till	Maliniec (Poland)	Stankowska and Stankowski (1988)
Gd-4581	22.3 ± 0.7	26.5 ± 1.3	dispersed organic matter in silt	Łeba Barrier (Poland)	Rotnicki and Borówka (1995)

* Calibrated using IntCal13 calibration curve (Reimer et al., 2013) with the Calib 7.0.4 software (Stuiver et al., 2017).

Table 2. Surface exposure ^{10}Be ages of pre-LLGM and LLGM erratic boulders in northern Poland. The list consists of 33 new exposure ages and 10 ^{10}Be ages recalculated from the original data of Rinterknecht et al. (2005, 2006). Densities of all samples (granitoids, granite gneisses and gneisses) were assumed at 2.7 g/cm^3. All ^{10}Be exposure ages are calculated with 'Lm' time-dependent scaling scheme for spallation according to Lal (1991) and Stone (2000) and global production rate according to Borchers et al. (2016).

Sample ID	Latitude DD	Longitude DD	Elevation (m a.s.l.)	Boulder perimeter/ height (m)	Boulder lithology	Sample thickness (cm)	Shielding factor[1]	Quartz (g)	Spike Be (g)	[^{10}Be] (10^4 at g^{-1})	Age (ka) ε = 1.3 (mm ka^{-1})	Age (ka) ε = 0 (mm ka^{-1})
Pre-LLGM erratics (Late Saalian)												
SAAL-01	51.9411	17.2008	122	9.7/1.3	granitoid	1.6	1.0000	18.38	0.1015	25.35 ± 0.81	57.9 ± 5.1	54.5 ± 4.5
SAAL-02	51.9410	17.2008	122	11.1/1.7	granitoid	1.2	0.9938	17.38	0.1018	27.76 ± 0.88	64.1 ± 5.7	59.8 ± 4.9
SAAL-03	51.9690	17.4716	120	9.5/1.1	granitoid	1.0	0.9975	16.00	0.1017	31.04 ± 1.00	72.2 ± 6.5	66.8 ± 5.5
SAAL-04	52.0883	18.3700	116	7.0/1.2	granitoid	2.5	1.0000	19.11	0.1005	10.30 ± 0.40	22.9 ± 2.0	22.3 ± 1.9
SAAL-05	52.1714	19.2166	138	8.8/1.4	granitoid	1.0	1.0000	17.09	0.1032	47.95 ± 1.51	115.2 ± 11.0	101.7 ± 8.5
SAAL-06	52.7110	19.9693	131	13.0/1.2	granitoid	1.0	1.0000	17.50	0.1019	7.58 ± 0.32	16.2 ± 1.4	15.9 ± 1.4
SAAL-07	53.2182	20.0510	157	9.5/1.9	granitoid	1.5	1.0000	15.23	0.1016	17.93 ± 0.79	38.3 ± 3.5	36.8 ± 3.2
LLGM ice marginal belts												
Leszno (Brandenburg) Phase												
											Mean ^{10}Be age (n = 6):	**20.7 ± 0.8**
LGM-01	52.3703	16.2724	99	8.7/0.8	gneiss	2.5	1.0000	15.53	0.1017	9.14 ± 0.50	20.5 ± 2.0	**20.1 ± 1.9^**
LGM-02T	52.1739	15.6817	133	6.0/2.0	granite gneiss	0.9	1.0000	15.01	0.1004	18.82 ± 0.60	41.3 ± 3.6	39.5 ± 3.3
LGM-02S	52.1739	15.6817	133	6.0/2.0	granite gneiss	1.1	1.0000	15.87	0.1019	27.74 ± 0.93	62.7 ± 5.6	58.6 ± 4.9
LGM-03	52.1185	15.6663	111	10.5/2.3	granite gneiss	2.2	1.0000	5.83	0.1021	8.91 ± 0.70	19.7 ± 2.2	**19.3 ± 2.1^**
LGM-04	51.9690	17.1330	120	13.5/1.2	granitoid	1.1	1.0000	18.32	0.1007	19.80 ± 0.63	44.4 ± 3.8	42.3 ± 3.5
LGM-05	51.9609	17.1492	111	10.4/1.3	granitoid	1.6	1.0000	17.98	0.1036	10.08 ± 0.50	22.3 ± 2.0	**21.8 ± 1.9^**
LGM-06	52.1457	18.3311	159	6.8/1.0	granitoid	1.4	1.0000	18.20	0.1024	25.08 ± 0.80	54.9 ± 4.8	51.7 ± 4.3
LGM-07	52.1303	18.3199	156	7.8/1.5	granitoid	1.3	1.0000	14.67	0.1024	21.31 ± 0.76	46.2 ± 4.1	43.9 ± 3.7
LGM-08	52.1511	18.3218	160	6.3/1.2	granitoid	1.6	0.9980	16.96	0.1019	30.68 ± 0.97	68.4 ± 6.1	63.6 ± 5.3
FRT-01	52.4411	15.0488	140	6.5/1.3	granitoid	0.8	1.0000	15.17	0.1024	10.13 ± 0.54	21.5 ± 2.0	**21.0 ± 1.9^**
FRT-02	52.3949	15.0943	133	7.0/0.8	granitoid	1.0	0.9981	14.91	0.1024	35.51 ± 1.22	82.2 ± 7.6	75.3 ± 6.3
FRT-03	52.4471	15.1529	161	10.1/1.8	granitoid	0.4	1.0000	15.95	0.1023	10.19 ± 0.72	21.1 ± 2.2	**20.6 ± 2.1^**
FRT-04	52.4489	15.1606	145	12.7/2.5	granitoid	2.5	1.0000	16.47	0.1036	11.96 ± 0.42	25.8 ± 2.2	25.1 ± 2.1
FRT-06	52.4426	15.2819	177	8.2/1.6	granitoid	1.2	0.9988	16.11	0.1032	10.45 ± 0.53	21.5 ± 2.0	**21.0 ± 1.9^**

Poznań (Frankfurt) Phase												**Mean ^{10}Be age (n = 14):**	**17.3 ± 0.5**
LGM-09	52.7390	19.6783	143	14.3/1.4	granitoid	1.0	1.0000	15.21	0.1036	15.93 ± 0.77	34.3 ± 3.2	33.0 ± 3.0
LGM-10	52.8749	19.6290	114	9.0/0.8	granitoid	1.0	1.0000	17.31	0.1021	7.95 ± 0.38	17.3 ± 1.6	**17.0 ± 1.5^**
LGM-11	53.4187	19.9013	166	9.5/1.2	granitoid	1.1	1.0000	14.68	0.1032	8.67 ± 0.47	17.8 ± 1.7	**17.5 ± 1.6^**
LGM-12	53.3874	19.5752	130	8.0/1.0	granitoid	1.2	1.0000	15.07	0.1026	11.50 ± 0.53	24.8 ± 2.3	24.1 ± 2.1
FRT-05	52.4897	15.1843	113	8.7/1.6	granitoid	1.1	1.0000	15.60	0.1023	14.13 ± 1.06	31.3 ± 3.5	30.2 ± 3.2
FRT-07	53.2823	17.5074	116	8.9/1.2	granitoid	1.0	1.0000	9.71	0.3080	8.91 ± 1.07	19.3 ± 2.8	**18.9 ± 2.7^**
FRT-08	52.9537	17.1255	89	17.5/2.2	gneiss	2.5	1.0000	15.03	0.1023	7.74 ± 0.43	17.5 ± 1.7	**17.1 ± 1.6^**
FRT-09	52.9525	17.3370	94	13.5/1.3	granitoid	1.2	1.0000	15.65	0.1025	7.66 ± 0.38	17.0 ± 1.6	**16.7 ± 1.5^**
FRT-10	52.7259	17.3231	105	20.5/1.1	granitoid	0.7	1.0000	16.46	0.1025	7.89 ± 0.65	17.3 ± 2.0	**16.9 ± 1.9^**
FRT-12	53.5238	16.2029	150	19.0/3.4	gneiss	1.6	0.9996	22.03	0.3049	9.81 ± 0.76	20.6 ± 2.3	**20.2 ± 2.2^**
FRT-13	53.6903	17.1372	171	20.5/1.9	gneiss	2.0	1.0000	9.29	0.3055	9.69 ± 0.57	20.0 ± 2.0	**19.5 ± 1.9^**
FRT-14	53.7271	17.1342	187	14.6/2.1	granitoid	2.5	0.9994	20.20	0.3052	8.55 ± 0.54	17.4 ± 1.7	**17.0 ± 1.7^**
LES-3	53.4806	20.2222	212	n.a./1.6	granitoid	2.0	1.0000	39.99	0.2500	3.45 ± 0.35	7.1 ± 0.9	7.0 ± 0.9
LES-4	53.4944	20.2389	172	n.a./1.8	granitoid	2.0	1.0000	40.00	0.2500	7.40 ± 0.54	15.8 ± 1.7	**15.5 ± 1.6*^**
LES-5	53.5792	20.0944	180	11.7/2.5	granitoid	2.0	1.0000	40.00	0.2500	19.24 ± 1.16	42.5 ± 4.3	40.6 ± 3.9*
LES-6	53.6006	20.0611	151	17.1/2.2	gneiss	2.0	1.0000	40.00	0.2500	8.08 ± 0.58	17.7 ± 1.9	**17.4 ± 1.8*^**
LES-7	53.6250	20.0417	132	13.0/2.8	granitoid	2.0	1.0000	60.51	0.2500	2.64 ± 0.33	5.8 ± 0.9	5.8 ± 0.8*
LES-8	53.5111	19.9000	255	4.5/1.1	granitoid	2.0	1.0000	40.00	0.2500	10.14 ± 1.10	20.1 ± 2.7	**19.7 ± 2.6*^**
LES-10	53.5764	19.9417	270	8.7/1.7	granitoide	2.0	1.0000	40.01	0.2500	6.78 ± 0.57	13.2 ± 1.5	13.0 ± 1.5*
LES-11	53.5222	19.8375	218	10.5/1.5	gneiss	2.0	1.0000	39.99	0.2500	7.94 ± 0.77	16.3 ± 2.0	**16.0 ± 2.0*^**
LES-12	53.5625	19.9528	275	10.1/1.6	granitoid	2.0	1.0000	40.01	0.2500	8.46 ± 0.70	16.4 ± 1.9	**16.1 ± 1.8*^**
LES-13	53.5528	19.9250	302	11.0/1.2	granitoid	2.0	1.0000	40.01	0.2500	19.15 ± 1.33	37.0 ± 4.0	35.5 ± 3.7*

All samples measured at the ASTER facility. AMS results are standardized to STD-11 (samples LGM and FRT) and SRM 4325 (samples LES). ^{10}Be/^{9}Be ratios were corrected for a process blank value of 6.08 x 10^{-12} (samples LGM and FRT-01 to FRT-10), 5.97 x 10^{-12} (samples FRT-11 to FRT-14), and 26.8 ± 1.4 x 10^{-12} (samples LES).

[1] Corresponding to self-shielding (direction and angle of surface dipping).

* Surface exposure ages recalculated from the original data of Rinterknecht et al. (2005, 2006).

^ Ages used in the error-weighted mean age calculation for the LLGM moraines.

n.a. – not available

Table 3. Bulk composition of sample FRT-11 before chemical treatment, analysed at the SARM-CRPG (Nancy, France) by ICP-OES (major elements), ICP-MS (trace element), atomic absorption (Li), colorimetry (B) and spectrophotometry (Cl).

Sample Name	SiO_2 %	Al_2O_3 %	Fe_2O_3 %	MnO %	MgO %	CaO %	Na_2O %	K_2O %	TiO_2 %	P_2O_5 %	LOI %	Total	Cl (ppm)	Li (ppm)	B (ppm)	Sm (ppm)	Gd (ppm)	Th (ppm)	U (ppm)
FRT-11	50.46	23.48	6.17	0.08	1.38	10.38	3.90	0.77	1.12	0.44	1.10	99.26	13	6.9	3.4	3.4	3.4	1.17	0.25

Table 4. Major element concentrations in sample splits after acid etching, which removed 14% of the sample, analysed at the SARM-CRPG (Nancy, France) by ICP-OES. Ca, K, Ti and Fe are target elements for the spallogenic/muogenic production of ^{36}Cl.

Sample name	SiO_2 %	Al_2O_3 %	Fe_2O_3 %	MnO %	MgO %	CaO %	Na_2O %	K_2O %	TiO_2 %	P_2O_5 %	LOI %	Total
FRT-11	51.52 ± 0.51	23.61 ± 0.23	4.56 ± 0.09	0.069 ± 0.007	0.99 ± 0.01	11.10 ± 0.22	4.04 ± 0.61	0.71 ± 0.04	1.43 ± 0.07	0.88 ± 0.18	0.59	99.51

Table 5. Surface exposure ^{36}Cl age of LLGM gabbro erratic with characteristics of FRT-11 sample. Sample and blank were spiked with a solution enriched in ^{35}Cl (99.9%). AMS measurements were normalized to in-house standard SM-CL-12, using an assigned value of 1.428 (± 0.021) x 10^{12} (Merchel et al., 2011), and assuming a natural ratio of 3.127 for the stable ratio $^{35}Cl/^{37}Cl$. The chemistry blank correction was performed by subtracting the number of atoms of Cl and ^{36}Cl in the blank from those in the sample.

Sample ID	Latitude DD	Longitude DD	Elevation (m a.s.l.)	Boulder perimeter/height (m)	Boulder lithology	Shielding factor	Sample thickness (cm)	Sample density (g cm^{-3})	Sample weight (g)	[Cl] (ppm)
FRT-11	52.8035	17.9141	107	13.1/2.9	gabbro	1.0000	1.9	3.0	48.75	101.7 ± 8.6

Sample ID	Mass of Cl in spike (mg)	$[^{35}Cl/^{37}Cl]$	$[^{36}Cl/^{35}Cl]$ (10^{-14})	Number of atoms Cl (10^{17})*	$[^{36}Cl]$ (10^4 atoms)*	$[^{36}Cl]$ (10^4 at g^{-1})	Excel® spreadsheet		CRONUScalc	
							Age (ka) ε = 1.3 (mm yr^{-1})	Age (ka) ε = 0 (mm yr-1)	Age (ka) ε = 1.3 (mm yr^{-1})	Age (ka) ε = 0 (mm yr-1)
FRT-11	1.601	4.470 ± 0.093	10.27 ± 0.64	842 ± 71	939 ± 81	19.0 ± 1.6	19.2 ± 3.0	20.1 ± 3.1	18.7 ± 2.9	20.0 ± 3.0
Blank	1.599	590 ± 16	0.447 ± 0.081	0.691 ± 0.063	12.3 ± 2.2	-	-	-	-	-

* Sample values are not yet corrected for blank.